Journal of Power Sources 196 (2011) 3604–3610

Contents lists available at ScienceDirect

Journal of Power Sources

journal homepage: www.elsevier.com/locate/jpowsour

Self-discharge behavior of polyacenic semiconductor and graphite negative electrodes for lithium-ion batteries

Kazuma Ohue[a], Takashi Utsunomiya[a,b], Osamu Hatozaki[b], Nobuko Yoshimoto[a], Minato Egashira[a], Masayuki Morita[a,*]

[a] Department of Applied Chemistry, Graduate School of Science and Engineering, Yamaguchi University, 2-16-1, Tokiwadai, Ube, 755-8611, Japan
[b] Subaru Technical Research Center, Fuji Heavy Industries Ltd., 9-6-3, Ohsawa, Mitaka, 181-8577, Japan

ARTICLE INFO

Article history:
Received 25 November 2010
Accepted 16 December 2010
Available online 24 December 2010

Keywords:
Graphite
Polyacene
Self-discharge
Open-circuit potential
Ac impedance

ABSTRACT

Variations in open-circuit potential (OCP) of artificial graphite and polyacenic semiconductor (PAS) negative electrodes have been investigated as a function of the storage time in alkylcarbonate-based electrolyte solutions after their cathodic charging (electrochemical lithiation) to discuss self-discharge phenomena of these negative electrodes for lithium ion batteries. The OCP of the graphite showed a plateau at ca. 90 mV vs. Li/Li^+ for a long period ($>8 \times 10^5$ s), which suggested the retention of a stage structure of lithiated graphite during the storage. The lithiated PAS electrode gave gradual changes in OCP during the storage in the carbonate-based electrolyte solutions, suggesting continuous loss of Li species in the electrode. Variations in the interfacial resistance determined by an ac method, corresponding to the changes in the structure and properties at the electrode/electrolyte interface, also showed different features for the lithiated graphite and PAS electrodes. The mechanisms of self-discharging for these carbonaceous electrodes are discussed from the results of the influences of temperature and additives on the OCP variations.

1. Introduction

There have been much efforts devoted to develop larger-sizes of lithium-ion batteries (LIBs) for electric vehicle (EV) and other stationary uses. One of the key issues for utilizing LIBs in such applications is ensuring the safety and reliability of the battery itself [1]. Self-discharge behavior of each electrode strongly influences not only the battery performances but also the safety issue of the total power system [2]. For example, when we use a negative electrode whose self-discharge rate is much faster than that of the counter positive electrode, float-charging of the cell under a constant voltage over a long period would cause serious overcharge at the positive electrode due to unbalancing the potential distribution. Thus, understanding the self-discharge behavior of each electrode has become more and more important to design and develop larger-sizes of LIBs [2].

With respect to graphite-based negative electrodes, for instance, Yazami and co-workers have reported the contribution of the self-discharge process to the capacity loss of the overall LIB system, and proposed self-discharge mechanisms deduced from their experimental results [3,4]. The main cause of the capacity loss of the negative electrode is considered to be certain chemical processes occurring at the electrode/electrolyte interface during the storage. Contribution of the SEI (solid-electrolyte-interphase) formation to the self-discharging processes is discussed in detail [3]. On the other hand, ageing mechanisms of oxide-based positive electrodes have also been investigated extensively [2,5,6]. However, there are few publications on the self-discharge characteristics for carbonaceous materials other than graphite. In the present work, we have examined a carbonized organic semiconductor material, so-called polyacenic semiconductor (PAS) [7], which has been used as high capacity negative electrodes for LIB [8,9] and electrochemical capacitors [10]. As PAS can store a larger amount of Li than graphite, it has been regarded as a high capacity negative electrode material of LIB. Despite of the well-established mechanism for the charge storage in PAS material [11,12], little has been understood on the capacity loss behavior of PAS during the long-term storage. In the present work, we have monitored the variation in the open-circuit potential (OCP) of PAS electrode in alkylcarbonate-based organic electrolyte solutions as a measure of self-discharging rate with storage time. The resulting OCP profiles as a function of the electrolyte composition were discussed with comparing those obtained for a lithiated graphite electrode.

2. Experimental

Powdered carbon, PAS (Kanebo) or artificial graphite (KS6, Timical) was used as the active material of the negative electrode. The

* Corresponding author. Tel.: +81 836 85 9211; fax: +81 836 85 9201.
E-mail address: morita@yamaguchi-u.ac.jp (M. Morita).

0378-7753/$ – see front matter © 2010 Elsevier B.V. All rights reserved.
doi:10.1016/j.jpowsour.2010.12.073

test electrode was composed of 90 wt.% (mass%) of the active material with 10 wt.% of a binder, poly(vinylidenedifluoride) (PVdF). It was made from slurry of the active material with the binder dispersed in *N*-methylpyrolidinon (NMP), which was coated on a Cu foil current collector. The thickness of the active material was controlled to ca. 70 μm. A laminate type three-electrode cell consisting of a PAS or graphite negative electrode as a test electrode was used in this work. Here, we used a lithium (Li) foil chip as a reference electrode and a large surface area Li foil as a counter electrode, in order to avoid possible influences of conventional positive electrode materials on the self-discharging behavior of the test electrodes. A geometric area of 6 mm × 6 mm was used as the working area of the test electrode. The electrolytic solution was 1 mol dm^{-3} (M) $Li(C_2F_5SO_2)_2N$ dissolved in mixed solvent of ethylene carbonate (EC) and diethyl carbonate (DEC) with 2:3 volume ratio (1 M LiBETI/EC + DEC). This electrolyte composition was chosen because of its compatibility with polymeric gel electrolytes containing the same solution composition [13,14]. An electrolyte system containing 5 wt.% of vinylene carbonate (VC) was also examined to discuss the effects of the SEI forming reagent in the solution. In this experiment, the base electrolyte composition of 1 M $LiPF_6$/PC (PC: propylene carbonate) was used to detect the effect of the additive more clearly. The water contents in these electrolyte solutions were less than 50 ppm. The total volume of the electrolyte solution in the cell was about 2 mL, the most of which were kept in the polypropylene separator sheets.

The charge and discharge cycling was carried out under a constant-current condition coupled with constant-potential (CC–CP) charging, where the term "charging" means the cathodic lithiation of the negative electrodes and "discharging" the anodic delithiation. Constant current rate of 80 mA g^{-1} was applied for charging and discharging of PAS and graphite. For PAS electrode, the cut-off conditions of charging were 800 mAh g^{-1} for the first charge and 600 mAh g^{-1} for the second charge under constant potential (0 V vs. Li/Li^+), each of which was done after the electrode potential reached at 0 V under the constant current charging. For the graphite (KS6) electrode, the charging capacity was set to 420 mAh g^{-1} for the first charge and 370 mAh g^{-1} for the second charge with the same current and potential conditions as those for PAS electrode. The same current density (80 mA g^{-1}) was employed for discharging the test electrodes with the cut-off potential of 2.5 V vs. Li/Li^+.

The open-circuit potential (OCP) of the negative electrode was monitored after each first or second charging. Variation in the potential was recorded for 10^6 s (ca. 280 h) at 25, 40 and 55 °C. An ac impedance method was applied to analyze the interfacial processes during the storage of the charged electrodes. As the measurement condition, ac amplitude of ±5 mV, frequency range from 20 kHz to 10 mHz, and no dc-bias (at rest potential, i.e. OCP) were employed. These electrochemical measurements were carried out under a dry Ar atmosphere.

3. Results and discussion

Typical charge and discharge curves of PAS and graphite (KS6) negative electrodes are shown in Fig. 1, which were obtained at the first two cycles in 1 M LiBETI/EC + DEC under a current rate of 80 mA g^{-1}. The potential profiles under the constant current conditions are typical for PAS [15] and artificial graphite [16]. The variation in the discharge potential at the graphite electrode reflected changes in its stage structure of lithiated graphite, i.e. graphite intercalation compound (GIC) [17,18]. The discharge capacity of ca. 320 mAh g^{-1} for the first cycle, which is almost the same as the ideal capacity of this material, indicates that the charging capacity of 420 mAh g^{-1} was enough to lithiate the graphite forming stage-1 GIC (LiC_6) and to compensate so-called irreversible

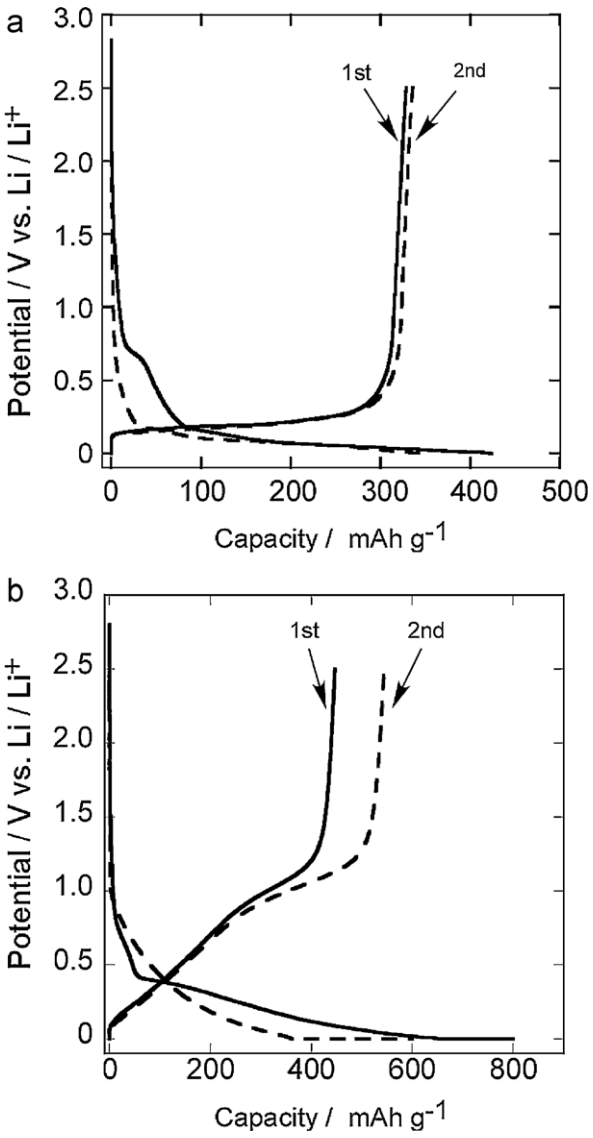

Fig. 1. Typical charge and discharge curves of graphite (a) and PAS (b) electrodes in 1 M LiBETI/EC + DEC at 25 °C.

capacity for the first charging of the graphite. On the other hand, the discharge capacity of PAS for the first cycle was ca. 450 mAh g^{-1}, which was much lower than the charge capacity (800 mAh g^{-1}), and tended to increase with the repeated cycle. This means that the present condition for the first charging process was not sufficient to compensate the irreversible capacity for the PAS electrode. In general, irreversible capacity in the first cycle of PAS is much higher than that of graphite, which also depends on the electrolyte composition.

In Fig. 2a, OCP of the graphite after the first charge (420 mAh g^{-1}) is plotted against the standing time. In the present work, the variations in OCP are shown for square root of time ($t^{1/2}$), which will be convenient to analyze when possible diffusion steps are included in the process concerning the self-discharge behavior of the electrode. The OCP value of the graphite changed to higher one immediately after the circuit was opened. After $t^{1/2} = 150\ s^{1/2}$, the potential kept almost constant at ca. 90 mV vs. Li/Li^+ for $t^{1/2} = 900\ s^{1/2}$ (ca. 225 h), which corresponds to the equilibrium potential of the reaction between stage I and stage II of GIC [17].

$$Li_{1-x}C_6 + xLi^+ + e = LiC_6 \quad (1)$$

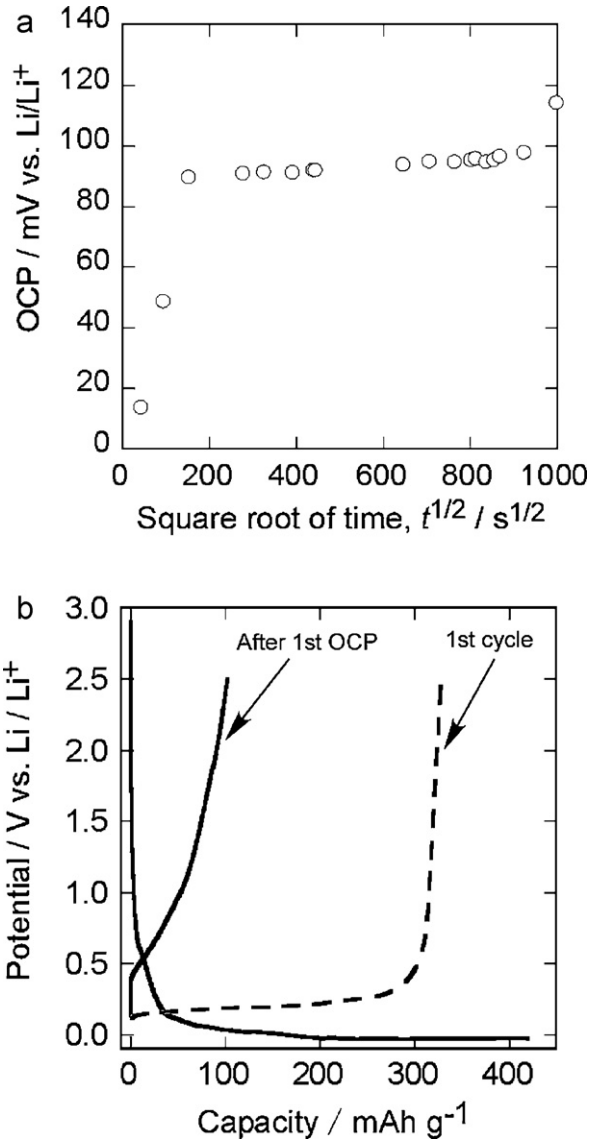

Fig. 2. Variation in OCP with time after the 1st charge (a), and the discharge curve after the OCP measurement (b) for graphite electrode in 1 M LiBETI/EC + DEC at 25 °C.

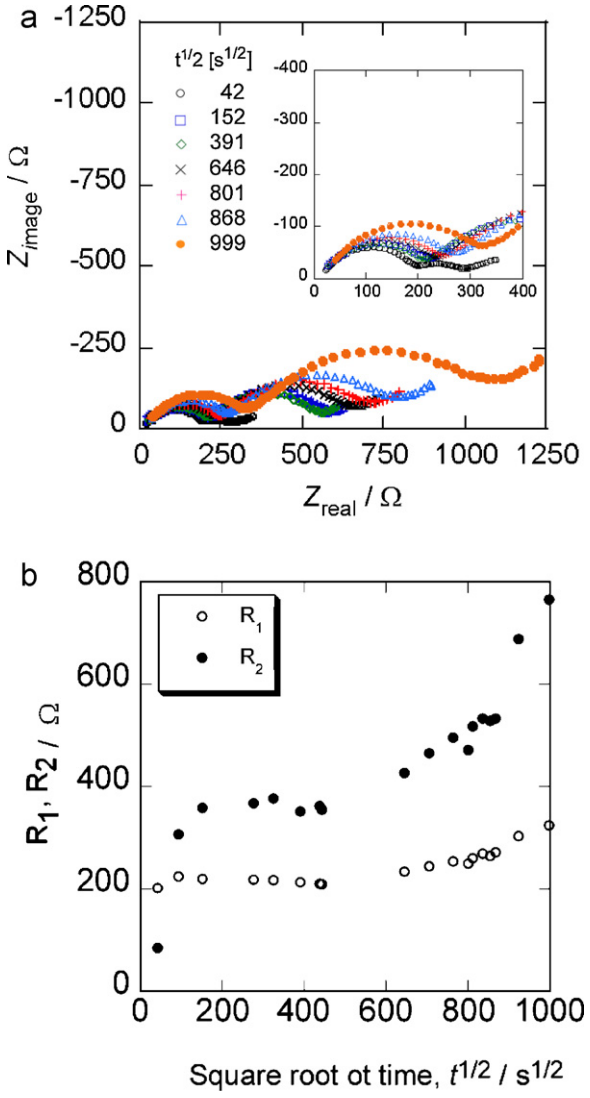

Fig. 3. Variations in the ac impedance with time after the 1st charge for graphite electrode in 1 M LiBETI/EC + DEC at 25 °C. (a) Nyquist plots, (b) variations in the resistance components in the impedance.

The OCP value increased steeply after $t^{1/2} = \sim 950$, which suggests that the GIC composition changed to another equilibrium state. Fig. 2b shows the discharge profile of the lithiated graphite after the storage for 10^6 s (ca. 280 h) at 25 °C, which is compared with that for the first discharge immediately after the full charge. The discharge capacity of ca. 100 mAh g^{-1} observed for the electrode after 10^6 s standing means that the changes in the OCP after the storage is caused by loss of Li species in the GIC structure.

Variations in the ac impedance responses for the lithiated graphite are shown in Fig. 3, as a function of the storage time after the first charge. The Nyquist plot of the impedance (Fig. 3a) consists of two semi-circles with Warburg component in the lower frequency region, which are characteristics for the lithiated graphite in organic electrolyte solutions [18]. In Fig. 3b, the resistance components of the semicircles in the higher and lower frequency regions, R_1 and R_2, are plotted with the storage time. Both resistances kept almost constant values with storage time after the first increase during $0 < t^{1/2} < 100$. The constant value of R_1 suggests the SEI resistance of the graphite unchanged up to $t^{1/2} \sim 600$. After that the film resistance increased gradually with the storage time. The increase in the R_2 value after $t^{1/2} \sim 600$ corresponds to the charge transfer resistance increasing with the self-discharge of the graphite electrode. These results qualitatively consist with those reported previously [18].

Fig. 4 shows a comparison in the OCP variation at different storage temperatures. The plateau potential did not change with the storage temperature. However, the time of the potential change from ca. 90 mV to higher one was slightly shortened with the increase in the storage temperature. The capacity retention during the storage was also decreased with the temperature. Thus, the OCP variation in Fig. 4 seems to correspond to the change in the self-discharging rate with temperature.

Fig. 5a shows the OCP variation of PAS electrode for the storage in 1 M LiBETI/EC + DEC at 25 °C. Although a similar profile was observed for the OCP after the first charge, here is employed the data after the second charge because of its better reproducibility. It gave a completely different profile from that of the graphite electrode. No stepwise change but continuous variation was observed for OCP throughout the storage time of 10^6 s. A similar OCP profile was obtained for the experiment using 1 M $LiPF_6$/PC as the electrolyte solution. In Fig. 5b, constant-current discharge curves are shown for PAS electrodes in LiBETI/EC + DEC before and after the storage. The discharge capacity of PAS electrode after the

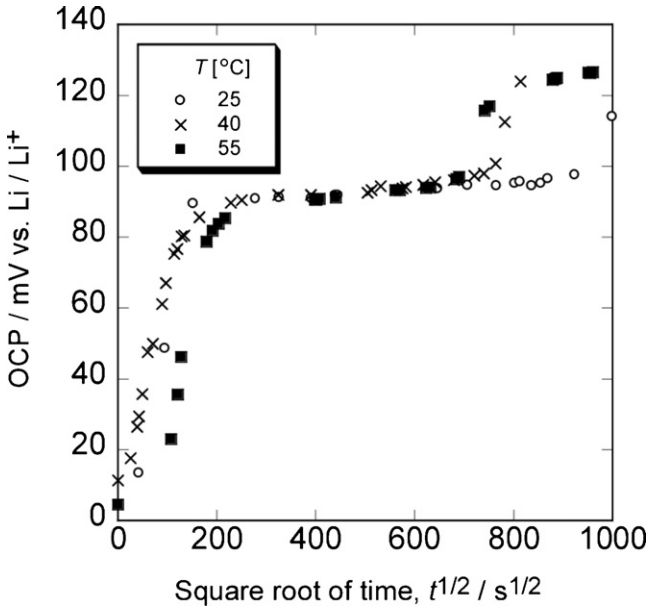

Fig. 4. Temperature dependence of the OCP variation with time for graphite in 1 M LiBETI/EC + DEC.

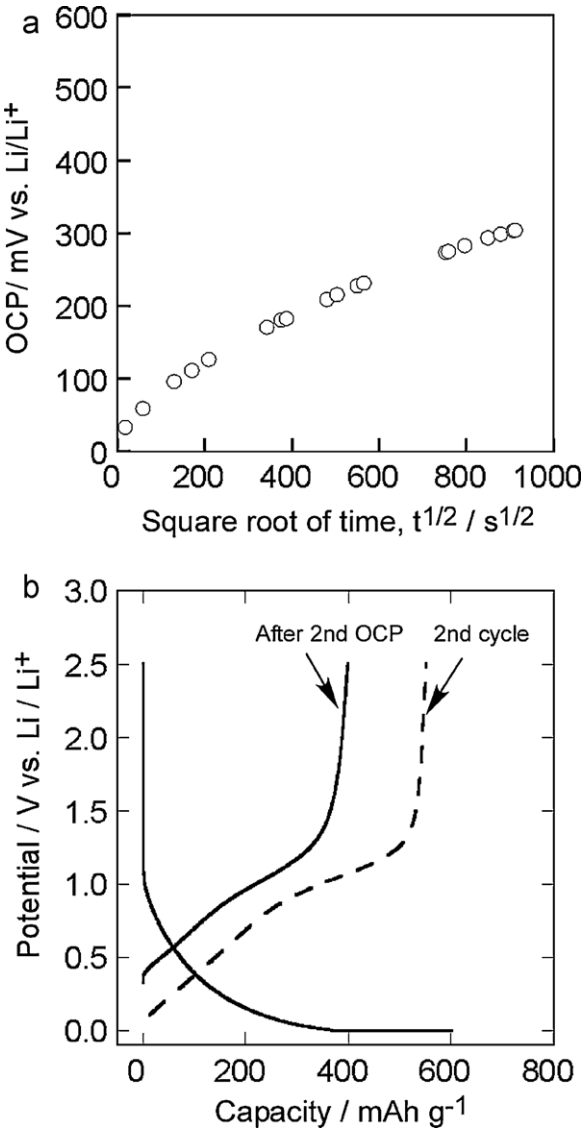

Fig. 5. Variation in OCP with time after the 2nd charge (a), and the discharge curve after the OCP measurement (b) for PAS electrode in 1 M LiBETI/EC + DEC at 25 °C.

2nd charge was about 520 mAh g^{-1}, which is reasonable value for the PAS electrode charged to 600 mAh g^{-1}. Storage for 10^6 s after the 2nd charge caused the capacity loss of about 120 mAh g^{-1}. Thus, the OCP change during the storage shown in Fig. 5a can be explained by the change in state-of-charge (SOC) of the PAS electrode. The OCP shown in Fig. 5a changed almost linearly with the square root of time ($t^{1/2}$), in which the slope of the line slightly changed with time. The potential of PAS electrode charged in the solution containing Li^+ is determined by the following reaction.

$$C_n + yLi^+ + ye = Li_yC_n \quad (2)$$

where n denotes the number of carbon consisting of unit PAS, and y the doping level of Li species. The maximum y/n ratio in PAS is generally about 1/2, which corresponds to the maximum charging capacity of about 1000 mAh g^{-1} [15]. Thus, the variation in OCP is regarded as the change in the doping level, y, of lithiated PAS. The discharge capacity after the 10^6 s storage (Fig. 5b), being less than that of fully charge PAS electrode by about 120 mAh g^{-1}, indicates that the change in OCP with the storage time is caused by the loss of Li-species in the lithiated PAS during the storage.

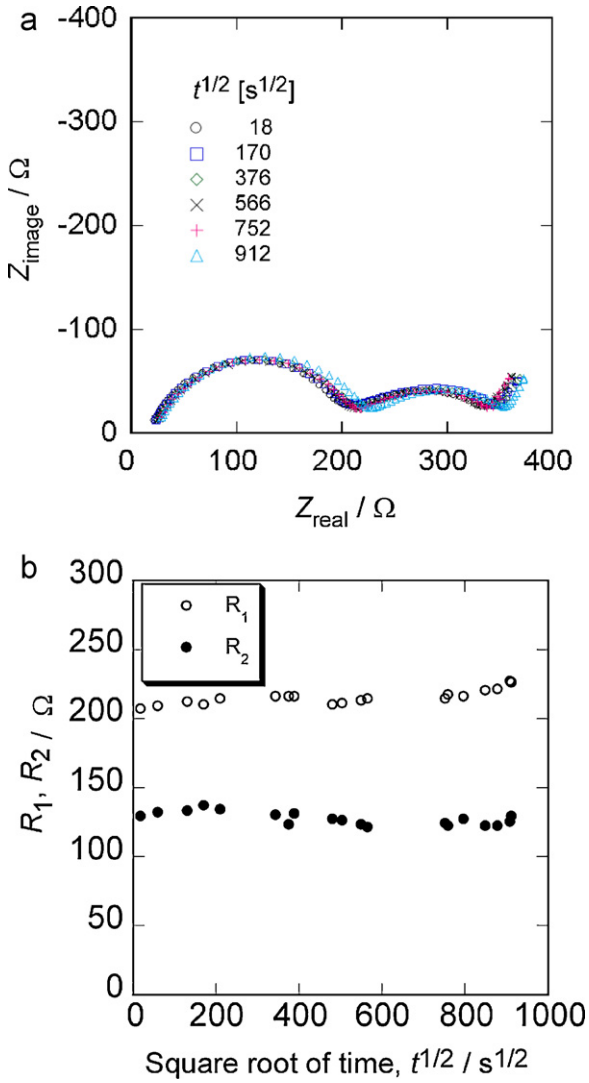

Fig. 6. Variations in the ac impedance with time after the 2nd charge for PAS electrode in 1 M LiBETI/EC + DEC at 25 °C. (a) Nyquist plots, (b) variations in the resistance components in the impedance.

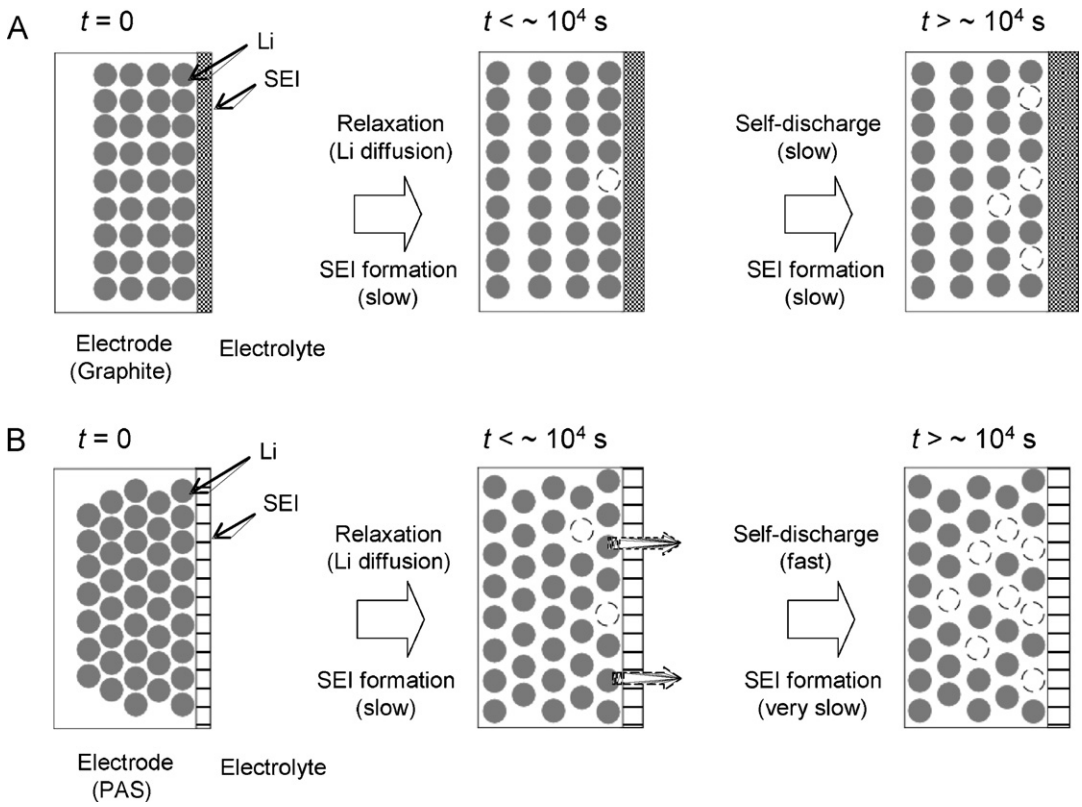

Fig. 7. Schematic models for self-discharging at graphite (A) and PAS (B) electrodes in alkylcarbonate-based electrolyte solution (LiBETI/EC + DEC) at 25 °C.

If the electrode potential of lithiated PAS in the electrolyte containing Li^+ is determined by a Nernst-type equation, the OCP value, E_{OCP}, will be determined by the concentration of Li^+ in the electrode:

$$E_{OCP} = E^\circ - \left(\frac{RT}{F}\right) \ln \left(\frac{[Li^+ \text{ in electrode}]}{[Li^+ \text{ in electrolyte}]}\right) \quad (3)$$

However, as shown in the discharge curves (Fig. 5b), the electrode potential of lithiated PAS gives almost linear change with the doping level (i.e. SOC), especially in the initial stage (highly doped level). A quasi-linear relation between OCP and square-root of storage time, $t^{1/2}$, shown in the initial stage of the storage (Fig. 5a) strongly suggests that the loss of Li species in the lithiated PAS is governed by some diffusion process. A slight change in the slope (or small bending of the curve) in the OCP vs. $t^{1/2}$ relation observed at around $t^{1/2} = \sim 600$ would be some changes in the process that lose active Li-species in the electrode.

Fig. 6 shows the results of the ac impedance measurement for lithiated PAS as a function of the storage time. The Nyquist plot of fully charged PAS electrode (Fig. 6a) was generally the same as that of the lithiated graphite, which consists of two semicircles. The charge transfer and interfacial resistances determined from the diameter of the semicircle did not show significant change with the storage time (Fig. 6b). Correlation between the continuous change (increase) of OCP with time and the constant values of the equivalent series resistance (ESR) for long-term storage suggests that the charge loss process of lithiated PAS does not cause the formation or growth of a resistive film on the electrode surface. From these results, we can conclude that the continuous increase in OCP of lithiated PAS during the storage is simply due to the loss of Li species in the electrode, without any significant changes in the surface chemistry of the electrode.

Fig. 7 shows qualitative expression for a possible self-discharge mechanism of lithiated PAS electrode during the storage at ambient temperature, comparing with that of charged graphite in organic electrolytes. For both electrodes, OCP changes observed in the initial period within $t < 10^4$ s are due to some relaxation of the concentration gradient of Li species in the solid that was more accumulated in the surface layer. After that, the self-discharge process becomes main factor of the OCP change. The main process of the self-discharge at the lithiated graphite would be the loss of charge (Li species in graphite) to form SEI at the electrode surface [2,18], while, at the lithiated PAS, the SEI formation would not be a major route of the self-discharge processes. Some heterogeneous reaction(s) between Li species in PAS and components in the electrolyte would be the main cause of the self-discharge, which leads to smaller changes in the interfacial resistance with the storage time.

Effects of the additive component in the electrolyte solution on the self-discharge characteristics of lithiated PAS are shown in Fig. 8. The OCP change in the PC-based electrolyte solution containing 5 wt.% VC (vinylene carbonate) as the additive is compared with that in the solution without VC (Fig. 8a). The slope of the OCP curve in the electrolyte with the additive was somewhat different from the solution without VC; the slope was rather steep at the initial period of the storage, while became smaller than that in the solution without VC after the storage time of 3×10^5 s (ca. $t^{1/2} \sim 550\,s^{1/2}$). The discharge capacity after the storage in the VC containing electrolyte, shown in Fig. 8b, was higher than that for the electrode stored in the solution without VC. These results would indicate that the additive VC reacts cathodically or chemically with lithiated PAS to form SEI at the electrode surface, which will contribute to decreasing further reaction of the Li species in the electrode to lose the stored charge.

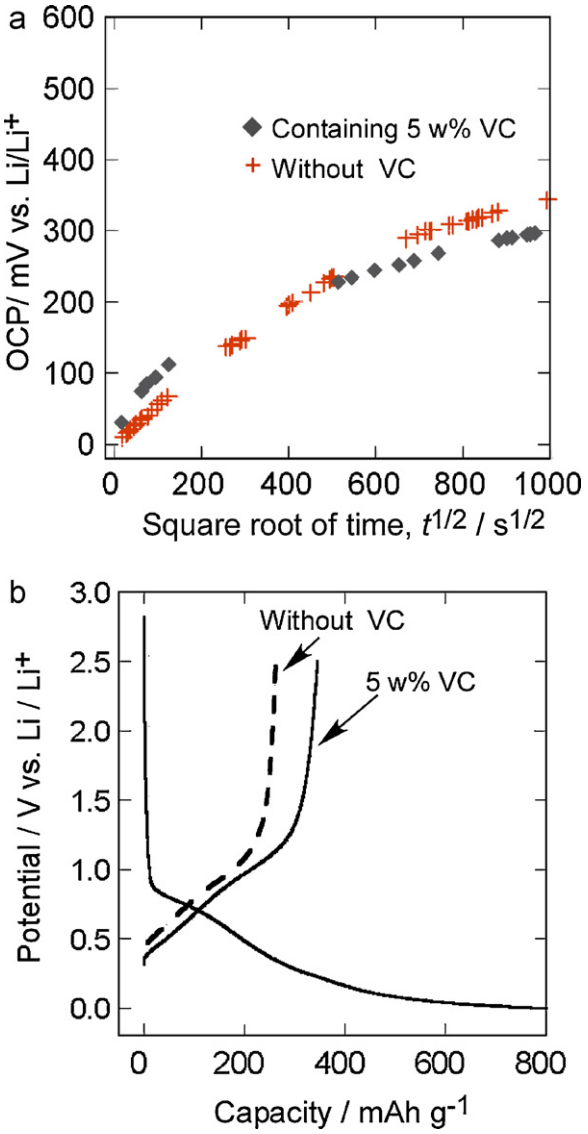

Fig. 8. Variation in OCP with time after the 1st charge (a), and the discharge curve after the OCP measurement (b) for PAS electrode in 1 M $LiPF_6$/PC with and without 5 wt.% VC at 25 °C.

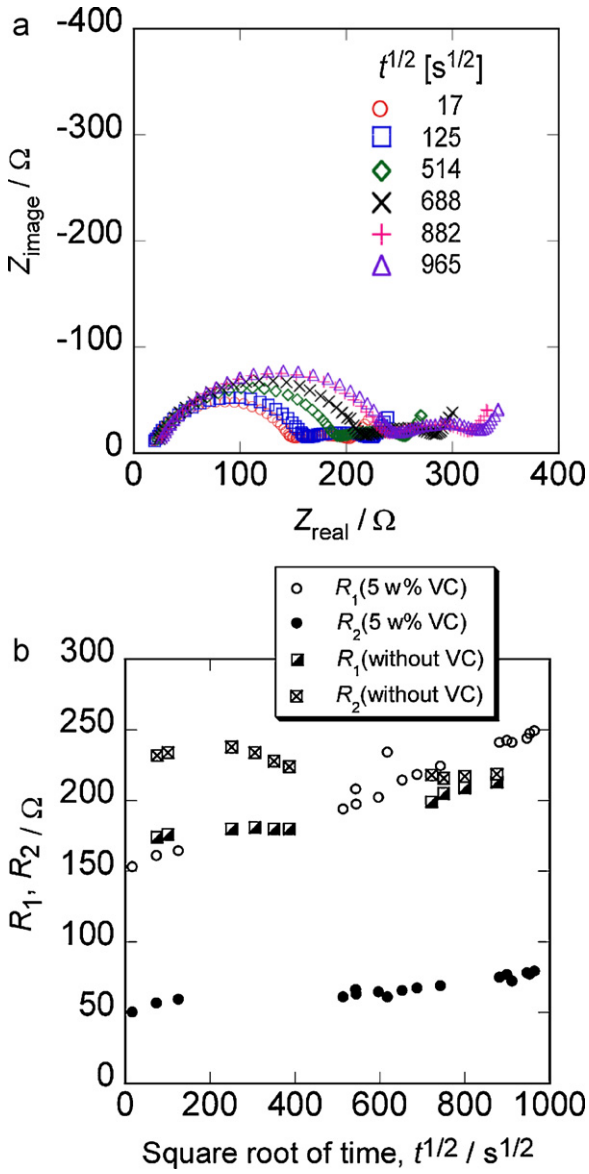

Fig. 9. Variations in the ac impedance with time after the 1 charge for PAS electrode in 1 M $LiPF_6$/PC with and without 5 wt.% VC at 25 °C. (a) Nyquist plots, (b) variations in the resistance components in the impedance.

Fig. 9a shows the results of the ac impedance measurements at PAS in the electrolyte containing VC. Two semi-circles were obtained in the complex plane, which are respectively related with the surface chemical and charge-transfer processes. When compared with the results shown in Fig. 6a, we can find that the impedance component in the lower frequency region was rather small in the electrolyte containing VC. In Fig. 9b, variations in the resistive components for each process at lithiated PAS in additive-free and VC containing electrolytes are plotted with the storage time. The interface resistance at higher frequency region, R_1, related with the SEI formation, showed a little difference between the cases with and without VC in the electrolyte. On the other hand, the charge-transfer resistance at lower frequency region, R_2, gave significant difference between the case with and without the additive in the electrolyte solution. Both of the absolute value of R_2 and its time dependence in the solution containing VC are smaller than that in the solution without the additive. These results suggest that the addition of VC in the PC-based electrolyte solution gives small influence on the resistance of SEI component itself, but contributes to the reduction in the charge-transfer resistance at lithiated PAS in the PC-based electrolyte.

Fig. 10 shows the OCP variations at lithiated PAS under different temperature conditions. The storage at higher temperature brought steep increase in OCP at the initial stage of the storage time. This would correspond to fast rate of the self-discharge of the charged electrode at higher temperature, which is generally observed. However, it is noteworthy that the OCP variation at higher temperature tended to saturate after the steep increase reached to around 300–400 mV vs. Li/Li^+. As the electrode potential is directly reflect to the amount of the Li species in the electrode, as discussed previously, this phenomenon implies that the self-discharging reaction at higher temperature (40–55 °C) will be limited after some extent of the reaction. That is, the film formation reaction, which is rather slow at the PAS electrode (Fig. 7), would be accelerated at higher temperature to form a thicker protective film, like as that formed on lithiated graphite, which will slow-down further self-discharging process.

Details in the effects of the electrolyte components and the storage temperature on the self-discharge characteristics of PAS and

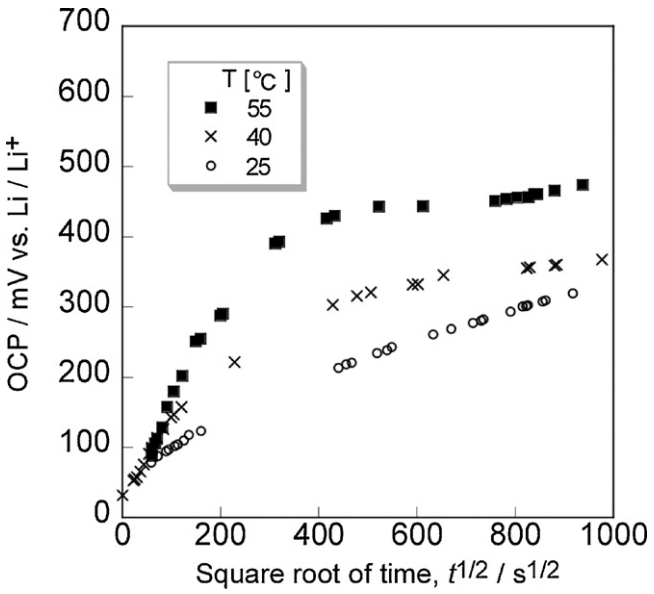

Fig. 10. Temperature dependence of the OCP variation with time for PAS in 1 M $LiPF_6$/PC. We employed a technique of monitoring the open-circuit potential of lithiated carbon electrodes with storage time to examine their self-discharge behavior in lithium-ion battery system, from viewpoints of ensuring the battery safety and reliability. We found clear differences in the self-discharge profile between graphite and polyacenic semiconductor electrodes, which were related with the differences in the properties of the surface layer formed during the storage.

graphite electrodes are now under investigation, whose results will be published elsewhere in near future.

4. Conclusions

The self-discharge behavior of a fully charged PAS electrode was examined by monitoring the open-circuit potential (OCP) as a function of the storage time, comparing with that of lithiated graphite. The OCP profile of charged PAS showed gradual changes with the storage time, while that of lithiated graphite gave a potential plateau over a long period. These potential changes corresponded to the changes in the state-of-charge (SOC), i.e. degree in self-discharging, of the electrodes. The ac impedance responses of the electrodes during the storage suggested that the self-discharge process at the graphite electrode is accompanied by such interfacial reactions as growth of the SEI layer. At the lithiated PAS electrode, however, the self-discharge process did not bring the increase in the interfacial impedance, but lead to the loss of Li species in the electrode. This difference in the self-discharging process between the graphite and PAS electrodes is considered to be based on the difference in the structures and properties of SEI formed on the electrodes.

Acknowledgement

This work was financially supported by Grants-in-Aid for Scientific Research (B) from JSPS (no. 21350101), for which the authors are most grateful.

References

[1] B. Scrosati, J. Garche, J. Power Sources 195 (2010) 2419.
[2] J. Vetter, P. Novák, M.R. Wagner, C. Veit, K.-C. Möller, J.O. Besenhard, M. Winter, M. Wohlfahrt-Mehrens, C. Vogler, A. Hammouche, J. Power Sources 147 (2005) 269.
[3] R. Yazami, Y.F. Reynier, Electrochim. Acta 47 (2002) 1217.
[4] M. Holzapfel, R. Alloin, Yazami, Electrochim. Acta 49 (2004) 581.
[5] M. Wohlfahrt-Mehrens, C. Vogler, G. Garche, J. Power Sources 127 (2004) 58.
[6] D. Aurbach, B. Markovsky, G. Saltra, E. Markevich, Y. Talyossef, M. Koltypin, L. Nazar, B. Ellis, D. Kovacheva, J. Power Sources 165 (2007) 491.
[7] T. Yamabe, M. Fujii, S. Mori, H. Kinoshita, S. Yata, Synth. Met. 145 (2004) 31.
[8] S. Yata, Y. Hato, K. Sakurai, T. Osaki, Synth. Met. 18 (1987) 645.
[9] B. Huang, R. Xue, G. Li, Y. Huang, H. Yan, L. Chen, F. Wang, J. Power Sources 58 (1996) 177.
[10] S. Yata, E. Okamoto, H. Satake, H. Kubota, M. Fujii, T. Taguchi, H. Kinoshita, J. Power Sources 60 (1996) 207.
[11] K. Tanaka, H. Ago, Y. Matsuura, T. Kuga, T. Yamabe, S. Yata, Y. Hato, N. Ando, Synth. Met. 89 (1997) 133.
[12] H. Ago, K. Tanaka, T. Yamabe, K. Takegoshi, T. Terao, S. Yata, Y. Hato, N. Ando, Synth. Met. 89 (1997) 141.
[13] N. Yoshimoto, A. Okamoto, M. Ishikawa, M. Morita, N. Ando, Y. Hato, Electrochemistry 71 (2003) 1049.
[14] N. Yoshimoto, A. Okamoto, M. Morita, N. Ando, Y. Hato, J. Power Sources 146 (2005) 195.
[15] S. Yata, Y. Hato, H. Kinoshita, N. Ando, A. Anekawa, T. Hashimoto, M. Yamaguchi, K. Tanaka, T. Yamabe, Synth. Met. 73 (1995) 273.
[16] J.R. Dahn, A.K. Sleigh, H. Shi, B.M. Way, W.J. Weydanz, J.N. Reimers, Q. Zhong, U. von Sacken, in: G. Pistoia (Ed.), Lithium Batteries—New Materials, Developments and Perspectives, Elsevier, 1994, p. 1.
[17] M Noel, V. Suryanarayanan, J. Power Sources 111 (2002) 193.
[18] R. Yazami, M. Deschamps, S. Genies, J.C. Frison, J. Power Sources 68 (1997) 110.